Available online at www.sciencedirect.com
ScienceDirect
Icarus 196 (2008) 506–517
ICARUS
www.elsevier.com/locate/icarus

Constraints on the composition of the martian south polar cap from gravity and topography

Mark A. Wieczorek

Institut de Physique du Globe de Paris, 4 Avenue de Neptune, 94107 Saint Maur des Fossés, France

Received 23 May 2007; revised 10 September 2007

Available online 10 January 2008

Abstract

The polar caps of Mars have long been acknowledged to be composed of unknown proportions of water ice, solid CO_2 (dry ice), and dust. Gravity and topography data are here analyzed over the southern cap to place constraints on its density, and hence composition. Using a localized spectral analysis combined with a lithospheric flexure model of ice cap loading, the best fit density of the volatile-rich south polar layered deposits is found to be 1271 kg m^{-3} with 1-σ limits of 1166 and 1391 kg m^{-3}. The best fit elastic thickness of this geologically young deposit is 140 km, though any value greater than 102 km can fit the observations. The best fit density implies that about 55% dry ice by volume could be sequestered in these deposits if they were completely dust free. Alternatively, if these deposits were completely free of solid CO_2, the dust content would be constrained to lie between about 14 and 28% by volume. The bulk thermal conductivity of the polar cap is not significantly affected by these maximum allowable concentrations of dust. However, even if a moderate quantity of solid CO_2 were present as horizontal layers, the bulk thermal conductivity of the polar cap would be significantly reduced. Reasonable estimates of the present day heat flow of Mars predict that dry ice beneath the thicker portions of the south polar cap would have melted. Depending on the quantity of solid CO_2 in these deposits today, it is even possible that water ice could melt where the cap is thickest. If independent estimates for either the dust or CO_2 content of the south polar cap could be obtained, and if radar sounding data could determine whether this polar cap is presently experiencing basal melting or not, it would be possible to use these observations to place tight constraints on the present day heat flow of Mars.

Keywords: Mars, polar caps; Geophysics

1. Introduction

The two polar caps of Mars are the largest reservoirs of easily accessible volatile deposits on the red planet. Besides playing a significant role in the present day martian climate, the discreet layers that make up the polar layered deposits are also a testament to past climate conditions that could span over more than one million years (for a review, see Clifford et al., 2000). At times of high obliquity, these volatiles could completely sublime, being transfered to more equatorial latitudes. If the polar deposits contained a significant quantity of CO_2, the release of this greenhouse gas could perhaps have given rise to more clement surface conditions (e.g., Jakosky et al., 1995).

Despite the importance of the martian polar caps in deciphering the volatile evolution of this planet, their bulk compositions remain poorly known. After seasonal deposits of CO_2 frost sublime from the northern cap, a perennial water-ice surface is revealed (e.g., Thomas et al., 1992) suggesting that at least this polar cap might be composed predominantly of H_2O. In contrast, the southern cap retains a yearly cover of CO_2 ice, opening the possibility that this deposit might harbor a non-negligible quantity of the largest constituent of the martian atmosphere. Recent observations suggest that the underlying layered deposits of the south polar cap are rich in water ice (Titus et al., 2003; Bibring et al., 2004), but the relative proportions of these two components remain unknown. Nevertheless, since CO_2 ice is significantly weaker than water ice, the present day morphology of the southern polar cap has been shown to be inconsistent with it being composed solely of dry ice (Nye et al., 2000).

E-mail address: wieczor@ipgp.jussieu.fr.

0019-1035/$ – see front matter
doi:10.1016/j.icarus.2007.10.026

In addition to water and dry ice, both polar caps are known to possess some quantity of dust (e.g., Langevin et al., 2005), some of which must be responsible for the prominent visible layering of these deposits. Near surface dust significantly affects the albedo of the polar deposits, and hence plays an important role in their thermal radiation balance (e.g., Kieffer et al., 2000; Kieffer and Titus, 2001). If a sublimation lag deposit of dust were to develop at times of high obliquity, this could perhaps act as a barrier to further volatile losses (e.g., Hofstadter and Murray, 1990; Mischna and Richardson, 2005). Dust could also have a significant affect on the rheological properties of ice. In excess of ∼10% dust by volume, the viscosity of ice increases, and this would lead to lower flow and internal deformation rates (Durham et al., 1992; Greve, 2000).

A question intimately related to the composition of the polar caps is whether they ever, or are currently, experiencing basal melting. As emphasized by Mellon (1996), the thermal conductivity of solid CO_2 is significantly less than that of water ice. Thus, as the concentration of CO_2 in the polar cap increases, so will its basal temperature, and under some circumstances it might be possible for either solid CO_2 or water ice to melt. If the polar caps grew to a thickness sufficient that they underwent basal melting, this could represent one important mechanism for recharging subsurface aquifers (Clifford, 1987), perhaps giving rise to a global groundwater system (Clifford, 1993; Clifford and Parker, 2001). As noted by Longhi (2006), this mechanism might have sequestered large quantities of atmospheric derived CO_2 in the underlying crust.

One manner to address the composition of the polar caps is to estimate their bulk density using knowledge of their gravity and topography signatures as measured from orbiting spacecraft. Since the densities of water ice, dry ice, and dust are distinctly different (∼920, 1560, and >2000 kg m^{-3}, respectively) such a measurement would place important constraints on the relative percentages of these three constituents. Using Viking-era data over the northern polar cap, Malin (1986) estimated that this deposit had a bulk density of about 1000 ± 500 kg m^{-3}. However, given the magnitude of the uncertainty, this estimate allows for a large range of volatile-rich compositions.

In this paper, the density of the south polar layered deposits is investigated using topography obtained from the Mars Global Surveyor mission (Smith et al., 2001a) and the most recent spherical harmonic model of the global gravity field (Konopliv et al., 2006). The gravity field is modeled using a lithospheric flexure model, and localized admittance and correlation spectra are used to infer its bulk density. Following a description of the analysis, two implications of this result are examined. First, the range of allowable compositions of the south polar cap are delineated, and these are shown to be consistent with the few independent constraints that are currently available. Second, since solid CO_2 has a large effect on the bulk thermal conductivity of the polar cap, the conditions under which present-day basal melting of either solid CO_2 or water ice could occur are explored.

2. Gravity and topography analysis

The gravity field of a planet is directly related to its internal distribution of mass. When combined with measurements of the planet's shape, as well as suitable assumptions based on geologic expectations, this allows for the possibility to invert for geophysical properties such as density and elastic thickness (for a review, see Wieczorek, 2007). Two standard analysis techniques are to investigate the relationship between these two observations in either the spatial or spectral (wavelength) domain. While both methods should in principle yield the same result, this study will use a spectral representation for two reasons. First, it is generally necessary to define a suitable load-free "reference" state of the two data sets in spatial analyses. However, since the volcanic load associated with the Tharsis province affects both the gravity field and topography globally (e.g., Phillips et al., 2001; Wieczorek and Zuber, 2004), it is necessary to either accurately model or remove this signature before attempting to analyze a specific region. Second, as discussed below, if noise and other unmodeled signals in the gravity field are uncorrelated with the surface topography, this will not bias an important cross-spectral measure of the two data sets.

2.1. Method

The approach utilized in this paper is to obtain cross-spectral estimates of the radial gravity and topography localized to a specific region on the surface of a spherical planet and to compare these with those of a similarly localized geophysical model. As described in detail by Wieczorek and Simons (2005, 2007), this is performed by multiplying the observed gravity g and topography f by a localization window h, and expanding the result in spherical harmonics to obtain the localized spherical harmonic coefficients Γ_{lm} and Φ_{lm}, respectively. Here, l and m are the spherical harmonic degree and order, respectively (with $|m| \leqslant l$), and the equivalent Cartesian wavelength is given by $\lambda \approx 2\pi R/\sqrt{l(l+1)}$, where R is the radius of the planet. The localized cross-power spectrum is defined as

$$S_{\Phi\Gamma}(l) = \sum_{m=-l}^{l} \Phi_{lm}\, \Gamma_{lm}, \tag{1}$$

from which one can construct the localized admittance

$$Z(l) = \frac{S_{\Phi\Gamma}(l)}{S_{\Phi\Phi}(l)}, \tag{2}$$

and correlation

$$\gamma(l) = \frac{S_{\Phi\Gamma}(l)}{\sqrt{S_{\Phi\Phi}(l) S_{\Gamma\Gamma}(l)}}, \tag{3}$$

functions, the latter of which is bounded to values between 1 and −1.

When a function on the sphere is multiplied by a localization window, the resulting power spectrum will differ from the non-windowed global spectrum. For the specific case where f and g are locally stationary stochastic processes, it has been shown that the expectation of the localized spectrum, the global

cross-power spectrum S_{fg}, and the power spectrum of the localization window S_{hh} are all related by a simple convolution-like relationship:

$$\left\langle S_{\Phi\Gamma}(l)\right\rangle = \sum_{j=0}^{L} S_{hh}(j) \sum_{i=|l-j|}^{l+j} S_{fg}(i)\left(C_{j0i0}^{l0}\right)^2, \tag{4}$$

where $\langle\cdots\rangle$ represents the expectation operator, L is the spherical harmonic bandwidth of h, and the symbol in parenthesis is a Clebsch–Gordan coefficient. This equation demonstrates that a localized spectral estimate at degree l is sensitive to the global power spectrum S_{fg} in the degree range $l \pm L$. Thus, in order to limit the leakage of power into a spectral estimate from degrees far from l, it is desirable to use a localization window with as small a bandwidth as possible.

In order to ensure that the spectral estimates are sufficiently localized in space, the amplitude of the localization window should be close to zero exterior to the region of interest. For this study, localization windows whose spatial power is optimally concentrated within a spherical cap of angular radius θ_0 and bandwidth L will be used (see Wieczorek and Simons, 2005, 2007; Simons et al., 2006, for details). After choosing the angular radius of the localization region, the spherical harmonic bandwidth will be chosen such that the best concentrated window contains more than 99% of its power in the region of interest (see Belleguic et al., 2005, for an example). Given the large bandwidths that are required to localize features as small as the south polar cap and the poor resolution of the martian gravity field, a multitaper analysis is not possible and only a single window will be used for each value of θ_0.

Before proceeding with the analysis, it is important to comment on how noise and other unmodeled signatures in the gravity field will affect both the admittance and correlation functions. The relationship between gravity and topography in the spectral domain can be written as

$$g_{lm} = Q_{lm}\, f_{lm} + I_{lm}, \tag{5}$$

where Q is a linear transfer function that describes a model relationship between the gravity and topography spherical harmonic coefficients, and I is that part of the signal not described by the model. When the signal I is uncorrelated with the topography f, such as would be the case if it were due to measurement noise, it is straightforward to show using Eq. (1) that the expectation of the cross-power spectrum S_{fg} will not be biassed by this signal. In contrast, the expectation of the power spectrum of the gravity field can be shown to be equal to

$$S_{gg}(l) = S_{gg}^{Q}(l) + S_{II}(l), \tag{6}$$

where S_{gg}^{Q} is the power spectrum resulting from the model Q, and S_{II} is the power of the signal not predicted by the model. Unmodeled signals will thus bias the power spectrum of the gravity field upwards, and as a result of the definition in Eq. (3), bias the correlation function downwards.

In this investigation, the relief and gravitational acceleration of the south polar region of Mars will be assumed to result from the emplacement of loads at the surface and the ensuing lithospheric deflection (see Section 2.2). The gravity and topography coefficients for such a model are related by a linear and isotropic transfer function Q_l, and in the absence of unmodeled signals, the correlation function is required to be identically unity for all spherical harmonic degrees. An observed value of the spectral correlation that is less than this would simply be interpreted as being a result of unmodeled gravitational signals that are uncorrelated with the topography. Under this assumption, the variance of the admittance at a given degree is directly related to the correlation function, which can be shown to be equal to

$$\sigma^2(l) = \frac{S_{\Gamma\Gamma}(l)}{S_{\Phi\Phi}(l)} \frac{1-\gamma^2(l)}{2l}. \tag{7}$$

Defining the "signal-to-noise ratio" to be equal to S_{gg}^{Q}/S_{II}, Eqs. (3) and (6) can be used to show that the correlation function will have a value of 0.707 and 0.816 when the signal strength is equal to, and twice that of, the "noise," respectively.

2.2. Analysis

The topography (Smith et al., 2001a) and radial gravity (JGM95J01; Konopliv et al., 2006) of the south polar region of Mars, here referenced to the surface of a flattened ellipsoid, are shown in Fig. 1. Since the gravity field is globally reliable to at most degree 75, the spherical harmonic representations used in generating both of these images have been truncated beyond this degree. The south polar layered deposits are clearly visible in the filtered topographic data, possessing elevations that reach up to about 4 km above the surrounding terrain. In contrast to the northern polar cap, the highest elevations are displaced approximately 3° equatorward from the rotation axis. The radial gravitational anomalies in this region are seen to be partially correlated in space with the topography of the polar cap, though, admittedly, the correlation is not perfect. A large factor contributing to this less-than-perfect correlation is noise in the gravitational model and the amplification of these errors by downward continuing this field to the surface. The correlation between gravity and topography will be seen later to be more significant in the spectral domain.

The relationship between gravity and topography will here be modeled using the flexure equation of a thin elastic spherical shell (e.g., Kraus, 1967; Turcotte et al., 1981). One major assumption of this analysis is that the surface relief of the south polar region of Mars is a combined result of the emplacement of a surface load onto a previously flat surface and the ensuing lithospheric deflection. The linear transfer function relating the gravity and topography spherical harmonic coefficients for this model is derived in Appendix A, and can be schematically written as

$$Q = Q(l, T_e, T_c, \rho_l, \rho_c, \rho_m, E, \nu), \tag{8}$$

where T_e is the elastic thickness, T_c is the crustal thickness, E is Young's modulus, ν is Poisson's ratio, and ρ_l, ρ_c and ρ_m are the load, crustal and mantle densities, respectively. The second major assumption of this analysis is that any portion of the gravity field that is not explained by this model is uncorrelated with

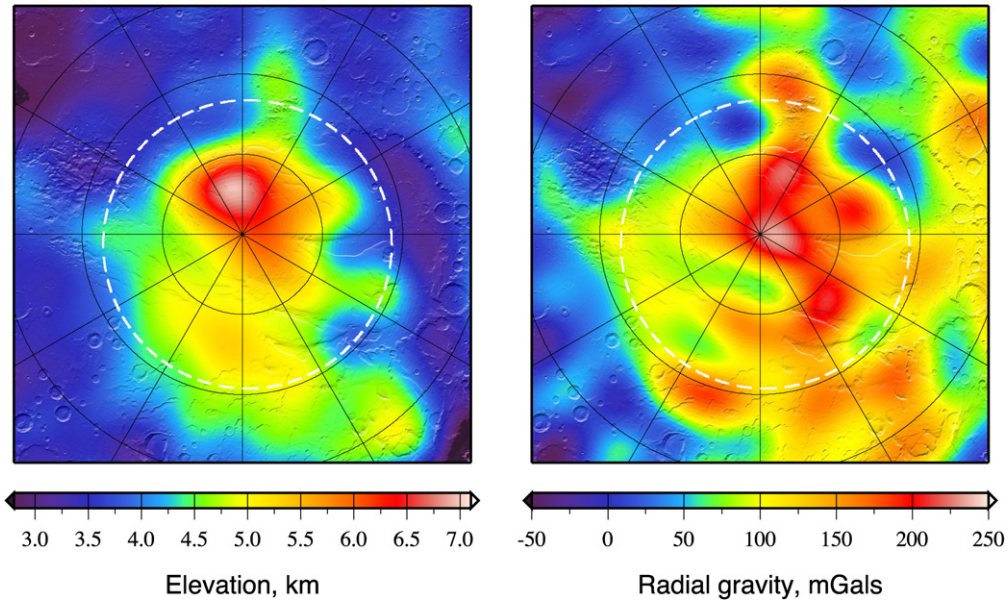

Fig. 1. Topography (MarsTopo719.shape; left) and radial gravity (JGM95J01; right) of the south polar region. Both images have been constructed using a maximum spherical harmonic degree of 75 and are referenced to the surface of a flattened ellipsoid that approximates the shape of Mars. The dotted circle with an angular radius of 9° corresponds to the region where the localized analysis was performed. Latitudinal grid lines in this polar stereographic projection are spaced every 5°, whereas longitudinal gridlines are spaced every 30°. For geologic context, both images are overlain by a shaded relief map.

the surface topography. Given that the relief of the south polar region is only a few kilometers, it is not necessary to use a finite-amplitude method (such as Wieczorek and Phillips, 1998) when calculating the gravitational anomalies.

Evidence in support of these assumptions comes from the Mars Advanced Radar for Subsurface and Ionospheric Sounding (MARSIS) experiment, which has mapped subsurface reflections beneath both the north and south polar caps (Picardi et al., 2005; Plaut et al., 2007). Prominent subsurface reflections that are coincident in depth with the surrounding terrain have been interpreted as representing the base of the polar layered deposits and variations in relief of the basal surface have been shown to be modest with respect to their thickness. (MARSIS data suggest that the maximum thickness of the south polar layered deposits is about 3.7 km.) The largest variations in basal relief are short-wavelength features that would not be detectable in the current model of the martian gravity field. In addition, there is no apparent correlation of this basal relief with the surface topography.

The following steps were used to calculate the localized admittance and correlation spectra over the south polar region. First, since the martian gravity field is only reliable globally to at most degree 75, the spherical harmonic representations of both the gravity and topography were truncated beyond this value. Next, for a given localization window, the average windowed radius of the surface was computed (this is simply the ratio Φ_{00}/h_{00}), and the gravity field coefficients were downward continued to this spherical surface. The radial gravity and topography were then expanded in the space domain, these functions were both multiplied by the same localization window, the resulting localized functions were expanded into spherical harmonics, and the localized admittance and correlation functions were finally computed. As a result of the windowing operation, only degrees less than $75 - L$ were analyzed (degrees larger than this have contributions from the unreliable gravity coefficients beyond degree 75). Furthermore, since the gravity signal associated with the Tharsis province has a disproportionate affect on the first 5 degrees of the martian gravity field (see Fig. 3 of Wieczorek and Zuber, 2004), only windowed spectra with degrees greater than $L+5$ were considered. Theoretical windowed admittance spectra were calculated in a similar manner by using Eq. (A.5) to generate synthetic gravity models.

A range of localization windows possessing angular radii between 8° and 12° were investigated. The optimal coordinates for the center of these windows were chosen by calculating localized correlation spectra on a grid centered over the south pole and then choosing that location were the average value of the correlation function was largest. Since the spectral bandwidth of the localization window increases with decreasing size, the smallest window with $\theta_0 = 8°$ and $L = 32$ yielded only a few useable localized spectral estimates. Although the boundary of this window confined a large portion of the polar layered deposits and excluded most of the surrounding rocky terrain, the small number of localized spectral estimates ensured that the inverted ρ_l and T_e possessed relatively large uncertainties. In contrast, while windows larger than $\theta_0 = 9°$ resulted in more spectral estimates to analyze, they invariably contained some contribution from the surrounding rocky terrain. As this ancient terrain certainly possesses a different density than the young polar deposits, it is possible that this signal could bias the results for the polar cap. As a compromise, as shown in Fig. 1, a localization window of $\theta_0 = 9°$ and $L = 28$ was chosen for this analysis.

The localized admittance and correlation spectra for this window are displayed in the left panel of Fig. 2. For degrees

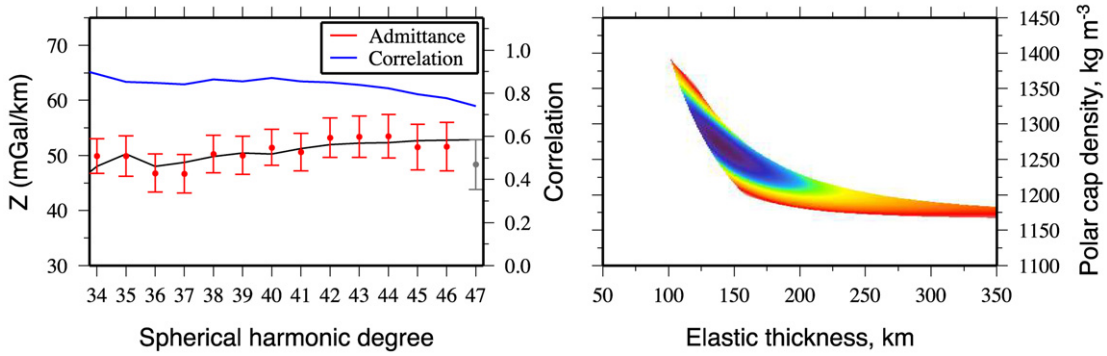

Fig. 2. (Left) Localized admittance (red) and correlation (blue) spectra obtained using a localization window with $\theta_0 = 9°$ and $L = 28$. Only degrees greater than $L + 5$ and less than or equal to $75 - L$ are shown, where L is the spherical harmonic bandwidth of the localization window. The admittance is plotted in light gray where the correlation function is less than 0.775, which corresponds to a signal-to-noise ratio of 1.5. The best fitting model with $\rho_l = 1271\ \mathrm{kg\,m^{-3}}$ and $T_e = 140$ km is shown in dark gray. (Right) Elastic thickness and load density parameter space that fits the admittance at all degrees to within 1-σ. Dark colors indicate a better fit.

less than about 43, the correlation spectrum is seen to possess values near 0.9, which corresponds to a signal-to-noise ratio of about 4. The correlation function slowly decreases beyond this degree, which is probably a result of the gradual loss of fidelity with increasing degree of the gravity model (the gravitational model JGM95J01 was biased towards a global power-law constraint beyond degree 59). Comparison with admittance and correlation spectra for different sized localization windows shows that the admittance function consistently decreases whenever the signal-to-noise ratio drops below 1.5, which corresponds to a spectral correlation of 0.775. For this reason, degrees where the correlation function was less than this value were excluded from further consideration. (It is noted that the signal-to-noise ratio for the northern polar cap is close to unity at all spherical harmonic degrees.)

Theoretical localized models of the gravity field were generated using Eq. (A.5), from which theoretical localized admittance functions were obtained. The load density and elastic thickness were treated as free parameters, whereas the other parameters were set to fixed values. The crustal thickness was assumed to be 50 km, Poisson's ratio was set to 0.25, Young's modulus was assumed to be 10^{11} Pa, and the crustal and mantle densities were chosen to be 2900 and 3500 $\mathrm{kg\,m^{-3}}$, respectively (e.g., Neumann et al., 2004; Wieczorek and Zuber, 2004). Given that the inverted elastic thickness was found to be rather significant, the results are not very sensitive to reasonable variations in these parameters.

The right panel of Fig. 2 shows that region of the elastic thickness and load density parameter space that can everywhere fit the observed admittance function within its 1-σ uncertainties. The ice cap density is constrained to lie between 1166 and 1391 $\mathrm{kg\,m^{-3}}$, possessing a best fit value of 1271 $\mathrm{kg\,m^{-3}}$. The best fit elastic thickness is 140 km, though it is noted that any value greater than 102 km can satisfy the observed constraints. The ice cap density is seen to be inversely correlated with the elastic thickness, and as the elastic thickness approaches infinity, the density approaches a minimum value of about 1175 $\mathrm{kg\,m^{-3}}$. Given the apparent lack of any regional flexure associated with the south polar layered deposits as determined by the MARSIS radar sounding data, Plaut et al. (2007) have estimated the present-day elastic thickness of the south polar region of Mars to be greater than about 150 km.

Similar analysis using both smaller and larger localization windows gave results that were not too different from those presented above. For the smallest localization window of 8°, the density was found to lie between about 1165 and 1520 $\mathrm{kg\,m^{-3}}$ and the elastic thickness was constrained to be larger than 93 km. For the slightly larger window of 10°, the limits on the density and elastic thickness were found to be 1140–1341 $\mathrm{kg\,m^{-3}}$ and >108 km, respectively. Even though the fit to the data was found to become increasingly poor for windows larger than 10°, results using larger windows are generally consistent with those of the smaller windows. Finally, it is noted that if one were to use a goodness-of-fit criterion where the root-mean-squared (rms) misfit was constrained to be less than or equal to the rms uncertainty of the observed admittances, the range of acceptable densities and elastic thicknesses would be somewhat greater. In particular, for a localization window of 9°, the limits of the density and elastic thickness would be 1119–1590 $\mathrm{kg\,m^{-3}}$ and >68 km, respectively. However, using this criterion, it should be noted that the best fitting theoretical admittances are systematically underestimated at low degrees, near perfectly fit at mid degrees, and overestimated at large degrees.

3. Discussion

3.1. Composition of the south polar layered deposits

The south polar layered deposits of Mars are likely to be composed of up to four major constituents: water ice, solid CO_2, dust, and perhaps CO_2 clathrate. As each of these components has a different density, it is possible to place constraints on their relative proportions using the measured density of the bulk assemblage. With four unknown quantities and one constraint, however, it is not possible to determine uniquely the relative proportions of all constituents. Since CO_2 clathrate has not as yet been detected anywhere on the martian surface, for simplicity, this component will initially be ignored, and the con-

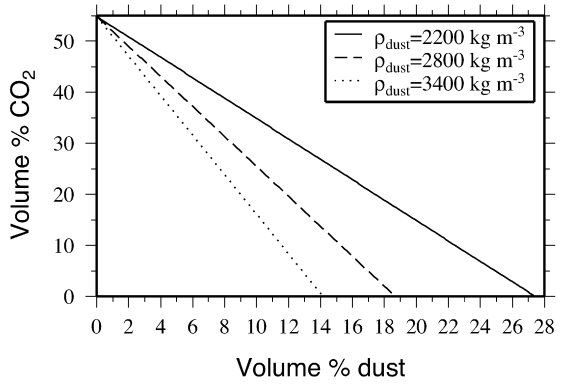

Fig. 3. Allowable concentrations of solid CO_2 in the south polar layered deposits as a function of dust content. The bulk density of the polar layered deposits is assumed to be 1271 kg m^{-3}, and results are plotted using three possible densities of martian dust.

sequences of its presence will be briefly addressed at the end of this section.

The density of water ice and solid CO_2 are here assumed to be 920 (e.g., Petrenko and Whitworth, 2002) and 1560 kg m^{-3} (e.g., Weast, 1986), respectively. Though the presence of any porosity in these materials would lower their bulk density, modeling of the densification of water-rich deposits at the north polar cap suggests that only the upper hundred or so meters would contain any appreciable pore space (Arthern et al., 2000). The density of martian dust is less well constrained. As one end member, dust on Mars might simply be mechanically comminuted crustal rocks. The highest reasonable density for this case would correspond to the mineral assemblages found in the basaltic martian meteorites, which have intrinsic densities of about 3400 kg m^{-3} (see Neumann et al., 2004). Alternatively, martian dust might be representative of aqueous and atmospheric alteration products, such as clays, zeolites, palagonites, and sulfates (e.g., Banin et al., 1992). A reasonable estimate for this end member is about 2200 kg m^{-3}.

If it were assumed that the south polar layered deposits were composed exclusively of water ice and solid CO_2, its bulk density implies that it must contain $45 \pm 18\%$ water ice by volume. If dust were an important component of the polar cap, given its greater density, the proportion of water ice would be even larger, possessing a value of 86% by volume for the largest assumed dust density. This trade-off is quantified in Fig. 3 where the permissible proportion of solid CO_2 in the south polar cap is plotted as a function of its concentration of dust. As to be expected, these two components are inversely correlated. For a dust free composition, the polar layered deposits would contain about 55% by volume solid CO_2. As the concentration of dust increases, the corresponding concentration of solid CO_2 decreases. For the end-member case where the polar layered deposits were completely free of solid CO_2, depending on the assumed density of dust, the dust content could lie between about 14 and 28% by volume.

These results indicate that the south polar layered deposits are volatile rich and that water ice is most likely the largest component. Three independent pieces of evidence that bear on the composition of these deposits are generally consistent with this conclusion. First, the MARSIS experiment has constrained the effective loss tangent of the south polar layered deposits, and if this is interpreted as being a result of dirty water ice, the dust concentration must be less than 10% by mass (Plaut et al., 2007), which corresponds to less than 5% by volume. Secondly, spectral reflectance data obtained from the imaging spectrometer OMEGA (Observatoire pour la Minérologie, l'Eau, les Glaces et l'Activité) on the Mars Express mission suggest that the materials underlying the carbon dioxide-rich perennial polar cap are largely composed of water ice (Bibring et al., 2004). While these spectra are only representative of the upper few millimeters of the surface and imply a large range of dust concentrations, it is conceivable that the purest end-member composition might be representative of the underlying deposits. The purest water-ice deposits appear to contain between 25 and 35% dust by mass (Douté et al., 2007), which corresponds to between 8 and 18% dust by volume (solid CO_2 is also required in some instances, though the amount was not quantified). In contrast, the nearly pure carbon-dioxide perennial deposits, which might only be about ten meters thick (Byrne and Ingersoll, 2003), appear to contain less than 1% dust by volume (Hansen et al., 2005; Douté et al., 2007). Lastly, since solid CO_2 is significantly weaker than water ice, Nye et al. (2000) have shown that the current morphology of the south polar cap is inconsistent with it being composed solely of dry ice. Unfortunately, that study did not place bounds on the permissible quantities of solid CO_2 that could be sequestered in this polar cap. Such a calculation would likely be strongly dependent on whether the CO_2 component was present as massive horizontal layers or inclusions in a predominantly water-ice matrix.

Finally, it is possible that CO_2 clathrate, $(CO_2)_{8-y}\cdot 46H_2O$ (Longhi, 2005), could contribute to the bulk composition of the south polar layered deposits. While this ice has not yet been detected from orbit, it is theoretically stable at the surface near the south pole under a limited range of temperatures. Furthermore, since the stability field of this ice greatly increases at even modest lithostatic pressures, wherever solid CO_2 and water ice were in contact, one would expect some quantity of clathrate to form (see Longhi, 2006). For typical concentrations corresponding to $y = 0$ to 1.5 (which is equivalent to hydration factors between 5.75 and about 7), the density of CO_2 clathrate at a representative temperature of 220 K should be between about 1090 and 1150 kg m^{-3} (using data from Udachin et al., 2001). Given the similarity in density of the south polar cap and CO_2 clathrate, it is theoretically possible that a large portion of this deposit could be composed of this material. Nevertheless, besides the lack of observational evidence for clathrates on Mars, it does not seem very probable that clathrates are volumetrically important in the south polar cap. As discussed by Longhi (2006), clathrates probably would not condense or precipitate from the atmosphere given its slow nucleation rate. In addition, while clathrate could form at the contacts between solid CO_2 and water ice, such a reaction rind would likely be volumetrically insignificant, especially if these two constituents were present as massive layers.

3.2. On the possibility of basal melting

The loss of heat from the interior of Mars to space should give rise to a nearly steady-state temperature gradient beneath the surface that is described by Fourier's law of heat conduction:

$$q = k(T)\frac{\mathrm{d}T}{\mathrm{d}z}, \tag{9}$$

where q is the heat flow, k is the temperature dependent thermal conductivity, and the last term is the temperature gradient. Because of this, it has long been recognized that the base of the martian polar caps could, under some circumstances, exceed the melting temperature of either water ice or solid CO_2 (e.g., Clifford, 1987; Mellon, 1996; Larsen and Dahl-Jensen, 2000; Longhi, 2006). If basal melting were to occur, this could contribute to the recharging of subsurface aquifers and potentially to the development of a global groundwater flow system (Clifford, 1993; Clifford and Parker, 2001). If the melting of solid CO_2 were important, this would be one manner to remove carbon dioxide from the atmosphere and to sequester it beneath the surface (Longhi, 2006). Evidence for past episodes of basal melting include the presence of inverted sinuous channels in the vicinity of the south polar cap that resemble terrestrial eskers (e.g., Kargel and Strom, 1992; Head and Pratt, 2001), although alternative interpretations of these features are possible (e.g., Tanaka and Kolb, 2001; Kolb and Tanaka, 2001).

Under the assumption of one-dimensional steady-state heat flow, all that is required to estimate the present-day basal temperature of the south polar cap is the current heat flow, the average surface temperature, and the depth dependence of the effective thermal conductivity. Of these, only the present-day average surface temperature of about 155 K is agreed upon. Nevertheless, by assuming that the polar layered deposits are composed of a mixture of water ice, solid CO_2, and dust, it is possible to model the effective thermal conductivity of the assemblage. Each of these components is, in general, temperature dependent, and the effective thermal conductivity will depend upon the manner in which the three components are mixed.

Fig. 4 shows the thermal conductivity of pure water ice as a function of temperature using the expression of Clifford and Parker (2001). This quantity is seen to have a moderate temperature dependence over the range of values that would likely be encountered in the south polar cap (from a surface temperature of 155 K to the melting temperature of about 273 K). Also shown is the thermal conductivity of solid CO_2 (Kravchenko and Krupskii, 1986), which, as previously emphasized by Mellon (1996), is about five times smaller than water ice. In the polar regions, some quantity of dust is likely to be present in both of these components as an intimate mixture. By treating dust as uniformly distributed spherical inclusions in a matrix of either water ice or solid CO_2, Maxwell's analytic formulation can be used to compute the effective conductivity of the assemblage. This model has been shown to be reasonably accurate when the volume fraction of inclusions is less than about 60% (Belova and Murch, 2004). Using this model, the

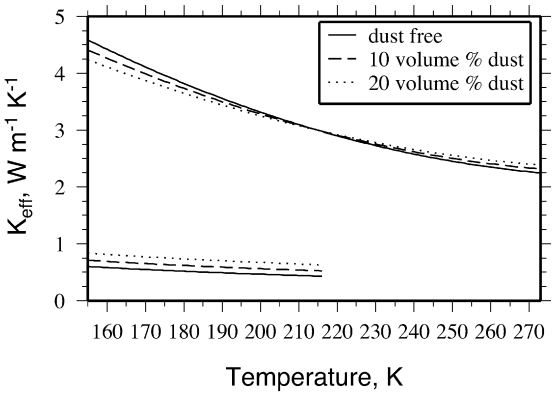

Fig. 4. Effective thermal conductivity of water ice (upper curves) and solid CO_2 (lower curves) as a function of temperature and dust content. The effective thermal conductivity was computed assuming that dust is present as spherical inclusions in a water-ice or solid-CO_2 matrix, and that the dust has a thermal conductivity of 3 W m^{-1} K^{-1}. Thermal conductivities are plotted from the average surface temperature of the south polar cap to the melting temperatures of water ice (∼273 K) and solid CO_2 (∼216 K).

expected temperature dependence of mixtures of water ice and solid CO_2 with 10 and 20% dust by volume are shown in Fig. 4 for an assumed dust conductivity of 3 W m^{-1} K^{-1}. As is seen, these volume fractions only modestly affect the thermal conductivity of the mixture. Although the thermal conductivity of martian dust is not well known, given its minimal impact on these calculations, other reasonable estimates would not give results that differed greatly from those presented here.

In order to determine if the polar cap could melt, it is simply necessary to integrate Eq. (9) from the surface to its base, and to compare the obtained temperature to the melting temperature of water ice (∼273 K) and solid CO_2 (∼216 K). For these calculations, it will be assumed that the bulk composition of the polar cap is uniform with depth, possessing a temperature-dependent effective thermal conductivity. In this manner, it is simple to determine the critical heat flow that is necessary to initiate melting as a function of the ice-cap thickness and bulk composition. While CO_2 clathrate will be neglected here, it is noted that this material should have a thermal conductivity very similar to solid CO_2 (see Waite et al., 2007). Hence, for the purpose of these calculations, the CO_2 component can be considered as the combined volume fraction of dry ice and clathrate.

Two end-member methods of mixing dirty water ice and dirty CO_2 will be considered. In the first model, it will be assumed that both of these components are present as interbedded horizontal layers (the thickness of the layers is irrelevant if they are uniformly distributed with depth throughout the polar cap). In this scenario, the effective thermal conductivity corresponds to the familiar "series" approximation. In the second model, it will be assumed that dirty CO_2 is present as spherical inclusions within a dirty water-ice matrix, and Maxwell's model will be used to calculate the effective thermal conductivity of the assemblage. While Maxwell's model is not strictly reliable when the volume fraction of inclusions is greater than about 60% (Belova and Murch, 2004), at higher volume fractions the model approximates the end-member scenario where the two components are treated as being in "parallel." Any reasonable

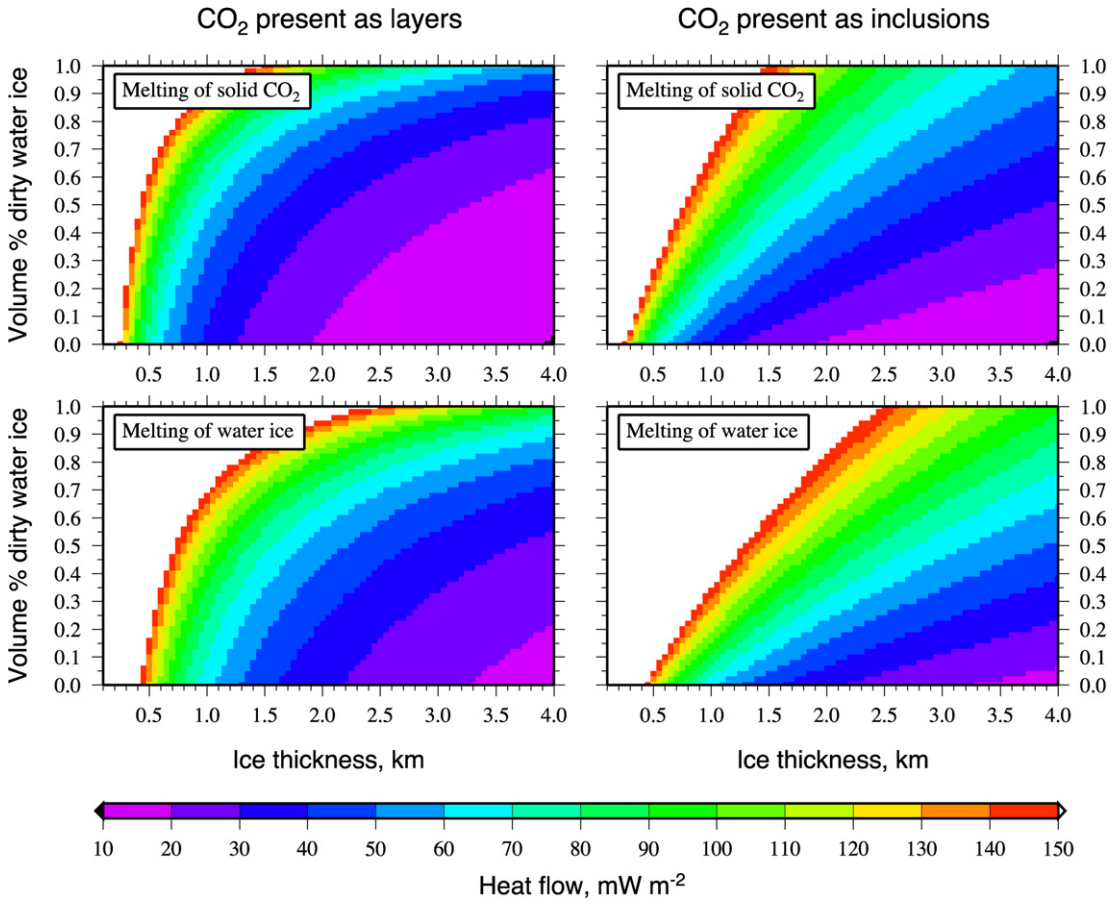

Fig. 5. Critical heat flow required to initiate melting at the base of the south polar layered deposits as a function of the ice cap thickness and its volume % dirty water ice. Upper row is for the melting of solid CO_2, and the lower row is for the melting of water ice. Left column corresponds to the situation where dirty-water and dirty-dry ice are present as interbedded horizontal layers, and the right column is for the case where dirty dry ice is present as spherical inclusions in a dirty water-ice matrix. The surface temperature is assumed to be 155 K, 10% dust is incorporated in both the water and dry ice, and the melting temperatures of water and dry ice are assumed to be 273 and 216 K, respectively.

structure of the polar cap will have an effective thermal conductivity between these two end members. The presence of 10% dust by volume will be assumed in these calculations, though it is noted that concentrations between 0 and 30% give nearly identical results.

The results of these calculations are presented in Fig. 5 where the critical heat flow required to initiate melting is shown as a function of ice-cap thickness and the volume fraction of dirty water ice. As determined in the previous section, the volume fraction of dirty ice in the south polar layered deposits should be in excess of about 45% by volume. Furthermore, thermal models based on the martian bulk silicate compositions of Wänke and Dreibus (1994) and Lodders and Fegley (1997) imply a present day heat flow of about 25 or 35 mW m^{-2}, respectively (e.g., Hauck and Phillips, 2002). Considering first the melting of solid CO_2, if water ice and solid CO_2 were present in the polar cap as interbedded horizontal layers, 10 to 25% CO_2 by volume would be sufficient to cause this constituent to melt where the polar cap is thickest (upper left panel). In contrast, if the CO_2 were present as spherical inclusions (upper right panel), more than about 40% by volume of this constituent would be necessary to initiate melting. Given that up to 55% solid CO_2 could be sequestered in the polar layered deposits, based on its bulk density, it seems probable that the basal melting of solid CO_2 could have occurred at some point in recent martian history.

The fate of any liquid CO_2 in the polar cap will depend upon its relative density with respect to the surrounding matrix. At pressures corresponding to 2 and 4 km below the surface of an ice-rich polar cap, liquid CO_2 at its melting temperature should have a density between 1180 and 1195 kg m^{-3}, respectively (see Lemmon et al., 2005). As this range lies within the uncertainty of the bulk polar cap density, liquid CO_2 might possess either positive or negative buoyancy. If the basal ices were dust poor, the residue after melting would be nearly pure water ice, and the liquid CO_2 would be negatively buoyant and sink. In contrast, if the basal ices were dust rich, liquid CO_2 would likely be close to being neutrally buoyant, and would not have any tendency to either rise or sink. In the case that liquid CO_2 was buoyant and rose, the surrounding matrix would become colder with increasing height above the base of the polar cap, and this would act to arrest any further upward melt migration.

The melting of water ice at the base of the martian polar caps is somewhat more difficult to achieve under present-day conditions. As seen in the lower left panel of Fig. 5, when combined with the high heat flow predictions of the Lodders and Fegley

(1997) model, the presence of more than 35% solid CO_2 by volume is required to achieve the necessary basal temperatures. It should be noted that in this scenario, the internal temperatures of the polar cap would have caused all of the CO_2 in its lower half to have melted (see also Longhi, 2006). Thus, in order to attain the same bulk composition, the upper half of the south polar cap would in fact be required to have a CO_2 concentration of more than 80% by volume. The case where solid CO_2 is present as spherical inclusions (lower right panel) is even less favorable for the melting of water ice at the base of the south polar cap.

The above considerations suggest that the melting of solid CO_2 at the base of the south polar cap can occur under conditions similar to those of the present. Water ice could even melt if the polar cap were dust poor and contained CO_2 concentrations in excess of ∼35%. Nevertheless, it should be emphasized that conditions in the past could have been much different than today and might have favored the scenario of basal melting. Higher surface temperatures, a higher heat flow, and a thicker polar deposit would all make it easier for basal melting to occur. In addition, if the polar cap were actively flowing, this could enhance the heat flow near its base.

4. Conclusions

An analysis of the spectral relationship between the radial gravity and topography of the martian south polar layered deposits show that their bulk density is 1271 kg m^{-3} with 1-σ limits of 1166 and 1391 kg m^{-3} and that the present-day elastic thickness in the surrounding region is greater than 102 km with a best fit value 140 km. Such a low value for the bulk density implies that these deposits are volatile rich, and that the largest component is most probably water ice. If the south polar cap is composed of a mixture of solid CO_2 and water ice, the CO_2 concentration by volume would be ∼55%. In contrast, if CO_2 were absent, then the concentration of dust could be anywhere between 14 and 28% by volume, depending on its assumed density.

While the thermal conductivity of the polar layered deposits is only modestly influenced by the permissible concentrations of dust, CO_2 can dramatically lower the bulk conductivity of the assemblage, and hence increase the interior temperatures of the polar cap. In the case where water and dry ice are present as interbedded horizontal layers, reasonable estimates for the present day heat flow imply that solid CO_2 would most likely melt where these deposits are thickest. If the CO_2 were instead present as inclusions in a water-ice matrix, basal melting of solid CO_2 could still be possible, but under more restrictive conditions. The basal melting of water ice beneath the thickest portions of the south polar cap is currently possible only if the high heat flow implied by the martian bulk silicate composition of Lodders and Fegley (1997) is assumed, and if water and dry ice in these deposit are present as horizontal layers. In this situation, all CO_2 would have melted from the lower half of the polar cap and the upper half would be required to be composed of about 80% CO_2 by volume.

These results demonstrate that there are currently two fundamental unknowns concerning the present-day state of the south polar layered deposits. First, in terms of estimating its bulk composition, a trade-off exists between the amount of CO_2 and dust that could be present. If CO_2 clathrate were present in volumetrically significant quantities, this constituent would only complicate matters. Secondly, in terms of the thermal state, these results are sensitive to whether water ice and solid CO_2 are present as massive horizontal layers, or if the solid CO_2 is present as inclusions in an ice-rich matrix. The rheological properties of the polar cap would also be dependent on how these two constituents are mixed. In particular, if solid CO_2 were present as interbedded horizontal layers, and if the polar cap was ever actively flowing, one might expect to find evidence for fold and boudinage structures.

Data from ongoing missions should be able to address some of these key issues. First, the analysis of radar sounding data from the MARSIS and SHARAD (SHAllow RADar; Seu et al., 2007) instruments onboard the Mars Express and Mars Reconnaissance Orbiter missions, respectively, are currently probing the subsurface structure of both the north and south polar layered deposits. From an analysis of the inferred loss tangents, it should be possible to place more precise constraints on their dust concentrations (Nunes and Phillips, 2006), from which it would then be possible to further constrain the amount of CO_2 that is present in the polar cap (see Fig. 3). Second, the continuing analysis of spectral reflectance data obtained from the instrument OMEGA on the Mars Express mission should be able to place further constraints on the composition and stratigraphy of ices that are perennially exposed in the polar regions (e.g., Douté et al., 2007). Finally, an improved static gravity field will be obtained from the Mars Reconnaissance Orbiter (Zuber et al., 2007a) that should enable an analysis of the admittance and correlation functions to much higher spherical harmonic degrees, especially over the south polar region. This should allow for a reduction in the uncertainty of the estimated bulk density of the south polar cap, as well a place tighter constraints on the elastic thickness. With a higher resolution gravity field, it might even be possible to place constraints on lateral variations in density of the polar layered deposits. Temporal variations in the gravity field might also be used to constrain the dust concentration of the seasonal CO_2 deposits (Smith et al., 2001b).

In concluding, it is noted that a better understanding of the south polar layered deposits could perhaps place constraints on the present day heat flow of Mars. As of yet, no direct measurement of this fundamental property has been made, even though it is critically important for understanding both the thermal and volatile evolution of this planet. As emphasized in Section 3.2, the temperature at the base of the polar layered deposits is highly dependent on the proportion of water and dry ice in these deposits, as well as the present day heat flow. If radar sounding data from either MARSIS or SHARAD could conclusively show that these deposits were currently undergoing basal melting, this would place strong constraints on the present day basal temperature. If independent estimates of dust concentration in these deposits could be obtained, this would place tighter

bounds on the permissible quantity of CO_2 that could be sequestered in the polar cap. With these constraints, it would be straightforward to determine the heat flow that is necessary to initiate basal melting of the polar layered deposits. If it could be conclusively shown that basal melting is not presently occurring, this constraint would give an upper bound on the present day heat flow.

Note added in proof

An improved gravity model of Mars that is based upon Mars Global Surveyor and Mars Reconnaissance Orbiter data has recently been constructed by Zuber et al. (2007b). This model yields slightly higher values for the localized correlation function over the south polar layered deposits, but does not permit the analysis of spherical harmonic degrees larger than those used in this analysis. For a localization window with an angular radius of 9°, this new gravity model (mromgm0020g) implies a best fit density of 1251 kg m^{-3} for the south polar layered deposits with 1-σ limits of 1157 and 1369 kg m^{-3}. The best fit elastic thickness is found to be 161 km, but any value greater than 110 km can fit the localized admittance function within its uncertainties. These updated values differ only marginally from those presented in the text and do not affect any of the implications. Using this same gravity model, Zuber et al. (2007b) also estimated the density of the south polar layered deposits using a method developed in the space domain combined with constraints on lithospheric flexure and ice thickness provided by MARSIS data. They obtained a concordant best fit density of 1220 kg m^{-3} for these deposits, with a 95% confidence interval of 740–1780 kg m^{-3}. For comparison, the 2-σ density limits from this spectral analysis are 1069 and 1626 kg m^{-3}.

Acknowledgments

The author thanks Klaus Mosegaard for his hospitality during a visit to the Niels Bohr Institute where most of this work was accomplished. This manuscript benefited from discussions with Christine Hvidberg and Francis Nimmo, as well as reviews by Greg Neumann and an anonymous reviewer. This is IPGP contribution 2282. All figures were created using the Generic Mapping Tools of Wessel and Smith (1991).

Appendix A. Polar cap admittance model

Consider the situation where the lithosphere of a planet, here approximated as a thin elastic spherical shell, is loaded at the surface by an infinitesimally thin mass sheet of surface density σ. Using the thin-shell flexure equation (e.g., Kraus, 1967), it can be shown in the spherical harmonic domain that the lithospheric deflection w_{lm} (here considered positive when directed upwards) is linearly related to the magnitude of the mass sheet σ_{lm} by the equation (Wieczorek, manuscript in preparation; for similar derivations see Turcotte et al., 1981; Willemann and Turcotte, 1981; McGovern et al., 2002)

$$w_{lm} = -C_l^0 \frac{\sigma_{lm}}{\rho_m}. \tag{A.1}$$

C_l^0 is a degree-dependent function that depends upon the elastic thickness T_e, Young's modulus E, Poisson's ratio ν, the crustal thickness T_c, and the mantle and crustal densities ρ_m and ρ_c, respectively. The superscript "0" of this function indicates that the load is placed at the surface. C_l^0 approaches zero both with increasing degree l and T_e, and possesses a value close to unity for long wavelengths and small T_e. The radial free-air gravitational acceleration at the surface is directly related to the mass anomalies associated with the surface deflection, the deflection of the crust–mantle interface, and the load itself, and can be shown to be equal to

$$g_{lm} = \frac{4\pi G(l+1)}{(2l+1)} \times \left[1 - C_l^0 \frac{\rho_c}{\rho_m} - C_l^0 \frac{\Delta\rho}{\rho_m}\left(\frac{R-T_c}{R}\right)^{l+2}\right]\sigma_{lm}, \tag{A.2}$$

where $\Delta\rho = \rho_m - \rho_c$. If the surface density σ is everywhere positive, as would be the case when material such as ice or lava is added on top of a previously flat surface, σ_{lm} can be approximated as being equal to the product of the load density ρ_l and thickness f^l. Expanding the load thickness into spherical harmonics and making use of Eq. (A.1), the equilibrium height of the surface is readily given by

$$f_{lm} = f_{lm}^l + w_{lm} = \frac{\sigma_{lm}}{\rho_l}\left(1 - C_l^0 \frac{\rho_l}{\rho_m}\right). \tag{A.3}$$

Combining Eqs. (A.2) and (A.3), the relationship between radial free-air gravity and surface topography can finally be expressed as

$$g_{lm} = Q_l f_{lm}, \tag{A.4}$$

where the linear transfer function is

$$Q_l = \frac{4\pi G\rho_l(l+1)}{(2l+1)}\left[\frac{1 - C_l^0 \frac{\rho_c}{\rho_m} - C_l^0 \frac{\Delta\rho}{\rho_m}\left(\frac{R-T_c}{R}\right)^{l+2}}{1 - C_l^0 \frac{\rho_l}{\rho_m}}\right]. \tag{A.5}$$

As both l and T_e increase, C_l^0 goes to zero, and Q approaches $2\pi G\rho_l$.

References

Arthern, R.J., Winebrenner, D.P., Waddington, E.D., 2000. Densification of water ice deposits on the residual north polar cap of Mars. Icarus 144, 367–381.

Banin, A., Clark, B.C., Wänke, H., 1992. Surface chemistry and mineralogy. In: Kieffer, H.H., Jakosky, B.M., Snyder, C.W., Matthews, M.S. (Eds.), Mars. Univ. of Arizona Press, Tucson, pp. 594–625.

Belleguic, V., Lognonné, P., Wieczorek, M., 2005. Constraints on the martian lithosphere from gravity and topography data. J. Geophys. Res. 110, doi:10.1029/2005JE002437. E11005.

Belova, I.V., Murch, G.E., 2004. Monte Carlo simulation of the effective thermal conductivity in two-phase material. J. Mater. Process. Technol. 153–154, 741–745.

Bibring, J.-P., Langevin, Y., Poulet, F., Gendrin, A., Gondet, B., Berthé, M., Soufflot, A., Drossart, P., Combes, M., Bellucci, G., Moroz, V., Mangold, N., Schmitt, B., and the OMEGA team, 2004. Perennial water ice identified in the south polar cap of Mars. Nature 428, 627–630.

Byrne, S., Ingersoll, A.P., 2003. A sublimation model for martian south polar ice features. Science 299, 1051–1053.

Clifford, S.M., 1987. Polar basal melting on Mars. J. Geophys. Res. 92, 9135–9152.

Clifford, S.M., 1993. A model for the hydrologic and climatic behavior of water on Mars. J. Geophys. Res. 98, 10973–11016.

Clifford, S.M., Parker, T.J., 2001. The evolution of the martian hydrosphere: Implications for the fate of a primordial ocean and the current state of the northern plains. Icarus 154, 40–79.

Clifford, S.M., Crisp, D., Fisher, D.A., Herkenhoff, K.E., Smrekar, S.E., Thomas, P.C., Wynn-Williams, D.D., Zurek, R.W., Barnes, J.R., Bills, B.G., Blake, E.W., Calvin, W.M., Cameron, J.M., Carr, M.H., Christensen, P.R., Clark, B.C., Clow, G.D., Cutts, J.A., Dahl-Jensen, D., Durham, W.B., Fanale, F.P., Farmer, J.D., Forget, F., Gotto-Azuma, K., Grard, R., Haberle, R.M., Harrison, W., Harvey, R., Howard, A.D., Ingersoll, A.P., James, P.B., Kargel, J.S., Kieffer, H.H., Larsen, J., Lepper, K., Malin, M.C., McCleese, D.J., Murray, B., Nye, J.F., Paige, D.A., Platt, S.R., Plaut, J.J., Reeh, N., Rice, J.W., Smith, D.E., Stoker, C.R., Tanaka, K.L., Mosley-Thompson, E., Thorsteinsson, T., Wood, S.E., Zent, A., Zuber, M.T., Zwally, H.J., 2000. The state and future of Mars polar science and exploration. Icarus 144, 210–242.

Douté, S., Schmitt, B., Langevin, Y., Bibring, J.-P., Altieri, F., Bellucci, G., Gondet, B., Poulet, F., and the MEX OMEGA team, 2007. South pole of Mars: Nature and composition of the icy terrains from Mars Express OMEGA observations. Planet. Space Sci. 55, 113–133.

Durham, W.B., Kirby, S.H., Stern, L.A., 1992. Effects of dispersed particulates on the rheology of water ice at planetary conditions. J. Geophys. Res. 97, 20883–20897.

Greve, R., 2000. Waxing and waning of the perennial north polar H_2O ice cap of Mars over obliquity cycles. Icarus 144, 419–431.

Hansen, G., Giuranna, M., Formisano, V., Fonti, S., Grassi, D., Hirsh, H., Ignatiev, N., Maturilli, A., Orleanski, P., Piccioni, G., Rataj, M., Saggin, B., Zasova, L., 2005. PFS-MEX observation of ices in the residual south polar cap of Mars. Planet. Space Sci. 53, 1089–1095.

Hauck, S.A., Phillips, R.J., 2002. Thermal and crustal evolution of Mars. J. Geophys. Res. 107, 1–19.

Head, J.W., Pratt, S., 2001. Extensive Hesperian-aged south polar ice sheet on Mars: Evidence for massive melting and retreat, and lateral flow and ponding of melt water. J. Geophys. Res. 106, 12275–12300.

Hofstadter, M.D., Murray, B.C., 1990. Ice sublimation and rheology—Implications for the martian polar layered deposits. Icarus 84, 352–361.

Jakosky, B.M., Henderson, B.G., Mellon, M.T., 1995. Chaotic obliquity and the nature of the martian climate. J. Geophys. Res. 100, 1579–1584.

Kargel, J.S., Strom, R.G., 1992. Ancient glaciation on Mars. Geology 20, 3–7.

Kieffer, H.H., Titus, T.N., 2001. TES mapping of Mars' north seasonal cap. Icarus 154, 162–180.

Kieffer, H.H., Titus, T.N., Mullins, K.F., Christensen, P.R., 2000. Mars south polar spring and summer behavior observed by TES: Seasonal cap evolution controlled by frost grain size. J. Geophys. Res. 105, 9653–9700.

Kolb, E.J., Tanaka, K.L., 2001. Geologic history of the polar regions of Mars based on Mars Global Surveyor data. II. Amazonian period. Icarus 154, 22–39.

Konopliv, A.S., Yoder, C.F., Standish, E.M., Yuan, D.-N., Sjogren, W.L., 2006. A global solution for the Mars static and seasonal gravity, Mars orientation, Phobos and Deimos masses, and Mars ephemeris. Icarus 182, 23–50.

Kraus, H., 1967. Thin Elastic Shells: An Introduction to the Theoretical Foundations and the Analysis of Their Static and Dynamic Behavior. Wiley, New York.

Kravchenko, Y.G., Krupskii, I.N., 1986. Thermal conductivity of solid N_2O and CO_2. Soc. J. Low Temp. Phys. 12, 46–48.

Langevin, Y., Poulet, F., Bibring, J.-P., Schmitt, B., Douté, S., Gondet, B., 2005. Summer evolution of the north polar cap of Mars as observed by OMEGA/Mars Express. Science 307, 1581–1584.

Larsen, J., Dahl-Jensen, D., 2000. Interior temperatures of the northern polar cap on Mars. Icarus 144, 456–462.

Lemmon, E.W., McLinden, M.O., Friend, D., 2005. Thermophysical properties of fluid systems. In: Linstrom, P.J., Mallard, W.G. (Eds.), NIST Chemistry WebBook, NIST Standard Reference Database Number 69. National Institute of Standards and Technology, Gaithersburg, MD. http://webbook.nist.gov.

Lodders, K., Fegley, B., 1997. An oxygen isotope model for the composition of Mars. Icarus 126, 373–394.

Longhi, J., 2005. Phase equilibria in the system CO_2–H_2O. I. New equilibrium relations at low temperatures. Geochim. Cosmochim. Acta 69, 529–539.

Longhi, J., 2006. Phase equilibrium in the system CO_2–H_2O: Application to Mars. J. Geophys. Res. 111, doi:10.1029/2005JE002552. E06011.

Malin, M.C., 1986. Density of martian north polar layered deposits—Implications for composition. Geophys. Res. Lett. 13, 444–447.

McGovern, P.J., Solomon, S.C., Smith, D.E., Zuber, M.T., Simons, M., Wieczorek, M.A., Phillips, R.J., Neumann, G.A., Aharonson, O., Head, J.W., 2002. Localized gravity/topography admittance and correlation spectra on Mars: Implications for regional and global evolution. J. Geophys. Res. 107 (E12), doi:10.1029/2002JE001854. 5136.

Mellon, M.T., 1996. Limits on the CO_2 content of the martian polar deposits. Icarus 124, 268–279.

Mischna, M.A., Richardson, M.I., 2005. A reanalysis of water abundances in the martian atmosphere at high obliquity. Geophys. Res. Lett. 32, doi:10.1029/2004GL021865. L03201.

Neumann, G.A., Zuber, M.T., Wieczorek, M.A., McGovern, P.J., Lemoine, F.G., Smith, D.E., 2004. Crustal structure of Mars from gravity and topography. J. Geophys. Res. 109, doi:10.1029/2004JE002262. E08002.

Nunes, D.C., Phillips, R.J., 2006. Radar subsurface mapping of the polar layered deposits on Mars. J. Geophys. Res. 111, doi:10.1029/2005JE002609. E06S21.

Nye, J.F., Durham, W.B., Schenk, P.M., Moore, J.M., 2000. The instability of a south polar cap on Mars composed of carbon dioxide. Icarus 144, 449–455.

Petrenko, V.F., Whitworth, R.W., 2002. Physics of Ice. Oxford Univ. Press, Oxford.

Phillips, R.J., Zuber, M.T., Solomon, S.C., Golombek, M.P., Jakosky, B.M., Banerdt, W.B., Smith, D.E., Williams, R.M.E., Hynek, B.M., Aharonson, O., Hauck II, S.A., 2001. Ancient geodynamics and global-scale hydrology on Mars. Science 291, 2587–2591.

Picardi, G., Plaut, J.J., Biccari, D., Bombaci, O., Calabrese, D., Cartacci, M., Cicchetti, A., Clifford, S.M., Edenhofer, P., Farrell, W.M., Federico, C., Frigeri, A., Gurnett, D.A., Hagfors, T., Heggy, E., Herique, A., Huff, R.L., Ivanov, A.B., Johnson, W.T.K., Jordan, R.L., Kirchner, D.L., Kofman, W., Leuschen, C.J., Nielsen, E., Orosei, R., Pettinelli, E., Phillips, R.J., Plettemeier, D., Safaeinili, A., Seu, R., Stofan, E.R., Vannaroni, G., Watters, T.R., Zampolini, E., 2005. Radar soundings of the subsurface of Mars. Science 310, 1925–1928.

Plaut, J.J., Picardi, G., Safaeinili, A., Ivanov, A.B., Milkovich, S.M., Cicchetti, A., Kofman, W., Mouginot, J., Farrell, W.M., Phillips, R.J., Clifford, S.M., Frigeri, A., Orosei, R., Federico, C., Williams, I.P., Gurnett, D.A., Nielsen, E., Hagfors, T., Heggy, E., Stofan, E.R., Plettemeier, D., Watters, T.R., Leuschen, C.J., Edenhofer, P., 2007. Subsurface radar sounding of the south polar layered deposits of Mars. Science 316, 92–95.

Seu, R., Phillips, R.J., Biccari, D., Orosei, R., Masdea, A., Picardi, G., Safaeinili, A., Cambell, B.A., Plaut, J.J., Marinangeli, L., Smrekar, S.E., Nunes, D.C., 2007. The SHARAD sounding radar on the Mars Reconnaissance Orbiter. J. Geophys. Res. 112, doi:10.1029/2006JE002745. E05S05.

Simons, F.J., Dahlen, F.A., Wieczorek, M.A., 2006. Spatiospectral concentration on a sphere. SIAM Rev. 48 (3), 504–536.

Smith, D.E., Zuber, M.T., Frey, H.V., Garvin, J.B., Head, J.W., Muhleman, D.O., Pettengill, G.H., Phillips, R.J., Solomon, S.C., Zwally, H.J., Banerdt, W.B., Duxbury, T.C., Golombek, M.P., Lemoine, F.G., Neumann, G.A., Rowlands, D.D., Aharonson, O., Ford, P.G., Ivanov, A.B., Johnson, C.L., McGovern, P.J., Abshire, J.B., Afzal, R.S., Sun, X., 2001a. Mars Orbiter Laser Altimeter: Experiment summary after the first year of global mapping of Mars. J. Geophys. Res. 106 (E10), 23689–23722.

Smith, D.E., Zuber, M.T., Neumann, G.A., 2001b. Seasonal variations of snow depth on Mars. Science 294, 2141–2146.

Tanaka, K.L., Kolb, E.J., 2001. Geologic history of the polar regions of Mars based on Mars Global Surveyor data. I. Noachian and Hesperian periods. Icarus 154, 3–21.

Thomas, P., Squyres, S., Herkenhoff, K., Howard, A., Murray, B., 1992. Polar deposits of Mars. In: Kieffer, H.H., Jakosky, B.M., Snyder, C.W., Matthews, M.S. (Eds.), Mars. Univ. of Arizona Press, Tucson, pp. 767–795.

Titus, T.N., Kieffer, H.H., Christensen, P.R., 2003. Exposed water ice discovered near the south pole of Mars. Science 299, 1048–1051.

Turcotte, D.L., Willemann, R.J., Haxby, W.F., Norberry, J., 1981. Role of membrane stresses in the support of planetary topography. J. Geophys. Res. 86, 3951–3959.

Udachin, K., Ratcliffe, C., Ripmeester, J., 2001. Structure, composition, and thermal expansion of CO_2 hydrate from single crystal X-ray diffraction measurements. J. Phys. Chem. B 105 (19), 4200–4204.

Waite, W.F., Stern, L.A., Kirby, S.H., Winters, W.J., Mason, D.H., 2007. Simultaneous determination of thermal conductivity, thermal diffusivity and specific heat in sI methane hydrate. Geophys. J. Int. 169, 767–774.

Wänke, H., Dreibus, G., 1994. Chemistry and accretion of Mars. Philos. Trans. R. Soc. London Ser. A 349, 2134–2137.

Weast, R.C., 1986. CRC Handbook of Chemistry and Physics, sixth ed. CRC Press, Boca Raton, FL.

Wessel, P., Smith, W.H.F., 1991. Free software helps map and display data. Eos 72, 441 and 445–446.

Wieczorek, M.A., 2007. Gravity and topography of the terrestrial planets. In: Spohn, T., Schubert, G. (Eds.), Treatise on Geophysics, vol. 10. Elsevier–Pergamon, Oxford, pp. 165–206.

Wieczorek, M.A., Phillips, R.J., 1998. Potential anomalies on a sphere: Applications to the thickness of the lunar crust. J. Geophys. Res. 103 (E1), 1715–1724.

Wieczorek, M.A., Simons, F.J., 2005. Localized spectral analysis on the sphere. Geophys. J. Int. 162, 655–675.

Wieczorek, M.A., Simons, F.J., 2007. Minimum-variance multitaper spectral estimation on the sphere. J. Fourier Anal. Appl. 13, 665–692.

Wieczorek, M.A., Zuber, M.T., 2004. Thickness of the martian crust: Improved constraints from geoid-to-topography ratios. J. Geophys. Res. 109, doi:10.1029/2003JE002153. E01009.

Willemann, R.J., Turcotte, D.L., 1981. Support of topographic and other loads on the moon and on the terrestrial planets. Proc. Lunar Sci. Conf. B 12, 837–851.

Zuber, M.T., Lemoine, F.G., Smith, D.E., Konopliv, A.S., Smrekar, S.E., Asmar, S.W., 2007a. Mars Reconnaissance Orbiter radio science gravity investigation. J. Geophys. Res. 112, doi:10.1029/2006JE002833. E05S07.

Zuber, M.T., Phillips, R.J., Andrews-Hanna, J.C., Asmar, S.W., Konopliv, A.S., Lemoine, F.G., Plaut, J.J., Smith, D.E., Smrekar, S.E., 2007b. Density of Mars' south polar layered deposits. Science 317 (5845), 1718–1719.